Forward scattering of light in thin opal films

S. G. Romanov*,† and C. M. Sotomayor Torres
Institute of Material Science and Department of Electrical, Information and Media Engineering, University of Wuppertal, Gauss-strasse 20, 42097 Wuppertal, Germany
(Received 29 October 2003; published 30 April 2004)

Angle-resolved spectra of the light scattered in a thin opal film have been measured behind the sample in three configurations, which differ by directions of the light incidence and detection. Two minima have been observed in scattering spectra and assigned to the attenuation by the (111) Bragg photonic bandgap along directions of the incident and detected photon flux. The irrelevance of the photonic bandgap minima to the actual path of scattered photon has been demonstrated. The projection of the directional (111) photonic band gap has been allotted to the plateau observed in the angle diagrams of the scattered light intensity. The spectra and the angle diagrams of the scattered light have been interpreted in terms of the weak scattering regime, when scattering serves for coupling a photon from one eigenmode of opal to another.

DOI: 10.1103/PhysRevE.69.046611 PACS number(s): 42.70.−a, 42.25.Fx, 78.35.+c

I. INTRODUCTION

If a collimated beam illuminates a three-dimensional (3D) photonic crystal (PhC), the flux behind it appears as a superposition of ballistic and scattered photons (Fig. 1). In the case of PhC of a finite thickness, the intensity of a ballistic flux is controlled by the Bragg attenuation length at diffraction resonance frequencies and by the photon mean free path (MFP) off the resonance. The ballistic component is transported by PhC optical eigenmodes, although not all available eigenmodes can be excited by a well-collimated beam. Scattered photons appear due to irregularities of the PhC lattice and they are transported by defect modes. Thus, the ballistic flux brings information about the photonic bandgap (PBG) structure, whereas the flux of scattered photons supplies the unstructured intensity background.

This model should be amended, if a sufficient part of scattered photons collides in average only once along their paths (Fig. 1). The corresponding concentration of defect modes is quite low and mode ensembles of perfectly crystalline and weakly disordered PhCs are alike, i.e., the central frequency and the width of a directional bandgap are nearly the same. In this case a photon will be coupled by a scattering event from one PhC eigenmode to another and moreover, this scattering will probe all PhC eigenmodes. The important consequence is that the weakly scattered light will also carry a fingerprint of the PBG structure. What sort of PBG-relevant information can be extracted from the scattered light is a subject of our interest. Obviously, the weak scattering regime becomes the multiple scattering one with the increase of the PhC thickness for the same defect density.

To some extent the weakly scattered light can be described in terms of radiation of a PhC-embedded isotropic light source. A convenient experimental realization of a point light source for PBG inspection is the insertion of a light emitter in a PhC; however, this method is useful only within the emission bandwidth. In contrast, the scattering approach is applicable over a whole spectral range of an external light source, although at the cost of a certain loss of the light intensity along all directions but the incident one.

A visualization of the 3D PBG of highly ordered colloidal crystals, stabilized in a liquid, was made in the ballistic propagation regime under illumination by a divergent monochromatic light beam [1], but this method fails when applied to dry colloidal crystals. Air-filled colloidal crystals assembled from dielectric spheres are known as opals [2]. The scattering at opal defects is stronger compared to that in liquid-stabilized colloidal crystals due to the higher refractive index (RI) contrast and denser sphere package. Hence, transmission measurements using a collimated beam comprise the main method to explore the light propagation in opals.

The choice of configuration for studies of the scattering is an important problem. On the one hand, the reflectance spectrum is formed near the opal surface (see, e.g., Ref. [3]) thus leaving the most of the sample volume unattended. Nevertheless, the anomalous coherent backscattering from opals was used to estimate the PBG width and the attenuation

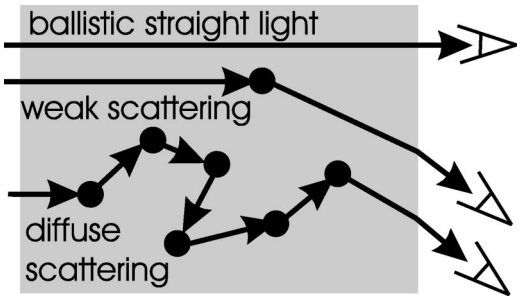

FIG. 1. Schematics of the straight ballistic and weakly and multiply scattered light detected behind a sample. The regime of weak scattering assumes one scattering event along the photon path as opposed to the diffuse scattering, when photons experience many collisions while crossing a slab.

*Corresponding author. FAX: (+49) (0)202 439-3037.
Email address: romanov@uni-wuppertal.de
†On leave from loffe Physical Technical Institute, 194021, St. Petersburg, Russia.

length [4]. On the other hand, the operation of PhCs as filter, superrefractive, or light emitting devices relies on propagating photons. Consequently, examination of the light scattering in the transmission configuration becomes the ultimate requirement.

So far, studies of light scattering in opals were carried out on bulk opals [5–7]. Moreover, to reduce the large inhomogeneous broadening of the diffraction resonance [5,6], opals were often infilled with a liquid of a RI, which nearly matches that of the opal carcass [5–7]. Reducing the RI contrast serves to increase the MFP, but changes the type of scatterers. For example, boundaries between randomly oriented $10-100$ μm size crystallites become main scatterers, which replace wavelength-scale defects dominating the scattering in air-filled opals. A resonant enhancement of the scattered light behind the opal slab, followed by a splitting of the transmission maximum with increasing Bragg attenuation, was reported in the case of the MFP matching the opal thickness [6], but these intriguing effects disappear in air-filled opals [8]. In current research-grade opals with a moderate RI contrast the MFP is limited to $5-20$ μm [4,9]; therefore, to reach the ballistic regime of photon propagation, opals of comparable thickness are necessary. Thin film opals are relatively novel materials [10], which possess much better crystallinity compared to bulk opals. Consequently, diffraction resonances in opal films show a much less inhomogeneous broadening [11,12]. Recently, we compared light extinction in air-filled bulk and thin film opals and showed that the resonant scattering on sphere vacancies, missed interstitials, dislocations, and other wavelength-scale defects dominates scattering in the latter in contrast to largely Rayleigh scattering on 10-nm scale fluctuations of the dielectric constant in the former [8].

The above arguments allow on to distinguish thin opal films as specific materials with respect to light propagation. The aim of this work is an experimental investigation of the forward-scattered light in opal films. The intensity of the light scattered in the forward direction in thin opal films in the weak scattering regime is studied as a function of wavelength and directions of light incidence and detection and compared with angle-resolved transmission spectra in the frequency range of the lowest frequency PBG. We discuss the observation of PBG features in scattering spectra obtained using different experimental configurations and deduce the directionality diagrams of the scattered light and demonstrate the PBG-induced modification of the scattering diagram. Characteristics of the scattered light were interpreted in terms of the ballistic propagation of photons generated by an effective point source placed inside a thin opal film.

II. EXPERIMENTAL TECHNIQUE

Opal films were prepared by drying a suspension of latex beads on hydrophilic glass slides [13]. They were assembled from beads of diameter $D=300\pm6$ nm and were crystallized in a face centered cubic (fcc) lattice with one set of (111) planes along the substrate. The film thickness was about 10 μm.

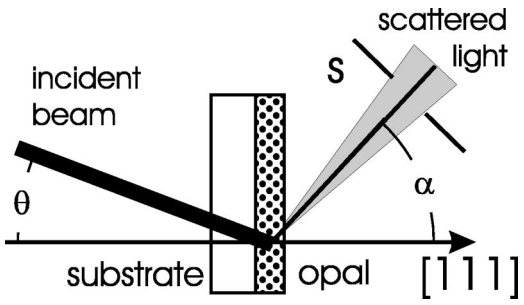

FIG. 2. Layout of scattering measurements excluding light refraction. θ is the angle of the beam incidence and α is the angle of the light detection, s is the aperture determining the light collection solid angle.

The opal films were illuminated by white light from a halogen tungsten lamp focused to a 1-mm-diameter beam. The orientation of the incident beam is indicated by the angle θ with respect to the [111] axis. Spectra of either the transmitted or scattered light were collected behind the film within the 5° solid angle along the direction defined by the angle α. The layout of the scattering configuration is shown in Fig. 2. Spectra of the scattered light were examined in three different configurations: (i) FS1 if the incidence beam propagates along the [111] axis ($\theta=0°$) and the angle α is a variable; (ii) FS2, if the angle θ is a variable and the detection direction is kept along the film normal ($\alpha=0°$); and (iii) FS3, if both angles are variables and $\theta=-\alpha$. The minus sign here denotes the clockwise direction of angle counting with respect to the film normal as opposed to the positive anticlockwise counting. In the transmission experiment both angles are variables and $\theta=\alpha$.

III. EXPERIMENTAL RESULTS

The evolution of FS1 scattering spectra with changing the detection angle α between 0 and 60° is shown in Fig. 3. The case of $\theta=\alpha=0°$ corresponds to the transmission spectrum along [111] axis of opal lattice with the well-defined minimum for the Bragg diffraction resonance (see e.g., Ref. [14]). Initially, increasing the detection angle from 0 to 20° leads to the decrease of the minimum bandwidth while preserving its relative depth. At $\alpha\geqslant20°$ (i) the minimum splits into two minima, each of them follows its specific angle dispersion, and (ii) the overall slope of the spectrum reverses its sign. In Fig. 4(a) the FS1 scattering spectrum is shown in comparison with two transmission spectra along directions of incidence and detection of the scattering spectrum. The good agreement of the central wavelengths of both minima in the scattering spectrum and diffraction resonances in transmission spectra suggests the common origin of these spectral features, namely, the diffraction on (111) planes. The dispersion of the angle-dependent minimum in the scattering spectrum coincides with that of the minimum in the transmission spectrum over the whole inspected range of angles and fits well the Bragg law $\lambda^2=(2d)^2(n^2-\sin^2\alpha)$, where $d=0.816\,D$ is the interplane distance along [111] axis [Fig. 4(b)]. The long wavelength minimum shows almost no variation of its cen-

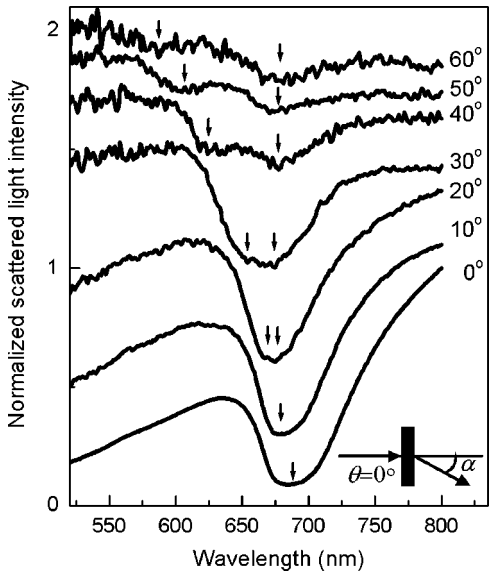

FIG. 3. Normalized FS1 scattering spectra as a function of the detection angle α. Numbers correspond to the detection angle. Spectra are shifted vertically for clarity. Arrows are a guide to the eye.

tral wavelength along the changing detection angle at $\alpha \geqslant 20°$. It is shifted to shorter wavelengths by about 3% with respect to the transmission minimum at $\theta=\alpha=0°$. Apparently, the angle range $0° < \alpha < 20°$, where FS1 spectra look

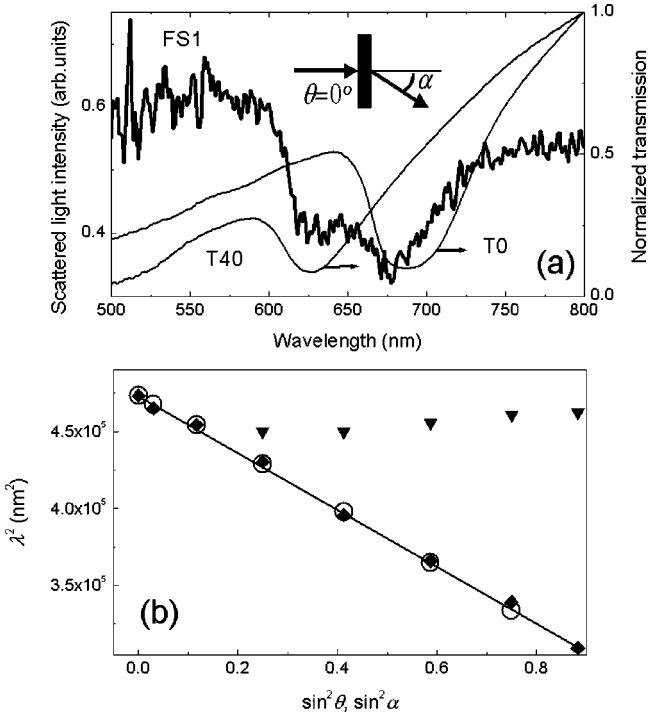

FIG. 4. (a) FS1 spectrum at $\theta=0°$, $\alpha=40°$ (thick line) and transmission spectra T0 ($\theta=0°, \alpha=0°$) and T40 ($\theta=40°, \alpha=40°$) (thin lines). (b) Angular dispersion of the (111) resonance in transmission as a function of the angle θ (open circles) and in FS1 scattering spectra as a function of the angle α. The long (short) wavelength resonances are indicated by triangles (rhombs). The line shows the Bragg law.

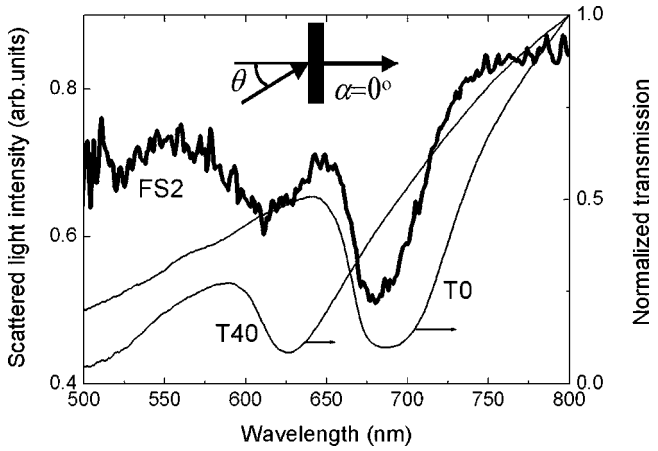

FIG. 5. FS2 spectrum at $\theta=40°$, $\alpha=0°$ (thick line) and transmission spectra T0 ($\theta=0°, \alpha=0°$) and T40 ($\theta=40°, \alpha=40°$) (thin lines).

alike, relates to the Bragg cone, which is the solid angle centered about the direction of the diffraction resonance and excluded from electromagnetic wave propagation at a given wavelength [15].

FS2 scattering spectra are similar to FS1 spectra, i.e., they display two minima. A comparison of these minima with respective transmission spectra (Fig. 5) demonstrates their close correspondence to transmission spectra obtained along directions of illumination and detection. The angular dispersions of both minima of FS1 and FS2 spectra are the same, whereas the geometrical optical paths of respective photons in the opal film are different.

The FS3 spectra support the observation of the insignificance of the actual optical path. If both incoming and outgoing fluxes sustain the same angle with respect to the [111] axis, there is only one minimum in the scattering spectrum, which is centered at the same wavelength as the Bragg resonance for this direction (Fig. 6). The total scattering angle, which is equal to 80° when $\theta=-\alpha=40°$, appears irrelevant, and only the parity of angles θ and α is important. These observations effectively link the scattering spectra to directions of the light incidence and detection.

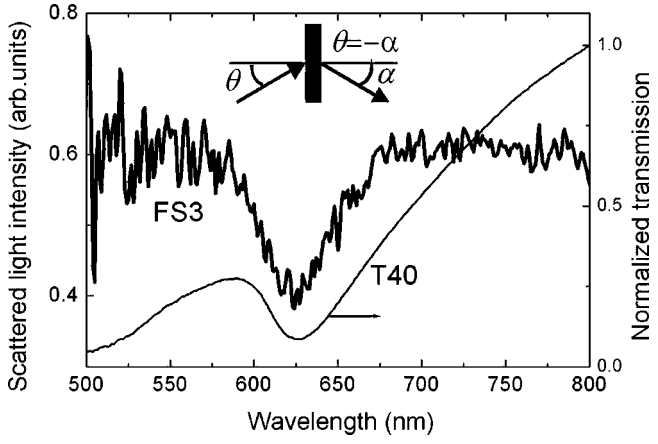

FIG. 6. FS3 spectrum at $\theta=40°$, $\alpha=-40°$ (thick line) and transmission spectrum T40 ($\theta=40°, \alpha=40°$) (thin line).

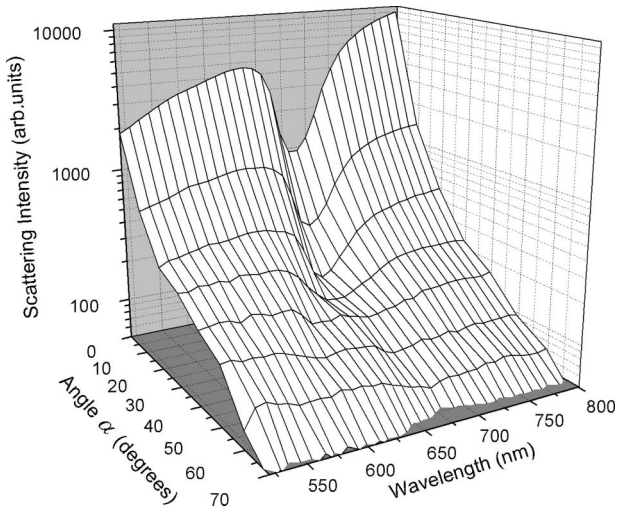

FIG. 7. Plot of the FS1 scattered intensity as a function of wavelength and angle α.

IV. DISCUSSION

The diffraction origin of the minima in the scattering spectra is proved by a comparison with transmission spectra. This test was designed as a result of simulations of the diffuse light in 2D PhCs [16], where the spectra of the straight light were separated from that of the diffuse light. The theory predicted a minimum in the scattered light spectra, which is positioned at 4–6 % shorter wavelengths as compared to the transmission minimum, which agrees well with our observations of the behavior of the nondispersive minimum [Fig. 4(b)]. However, the angle averaging made for diffuse light spectra [16] barred the appearance of the angle-dispersive minimum in simulations.

Further insights into the PBG effect upon the scattering require the analysis of the scattered light intensity. The FS1 configuration readily lends itself for this analysis because the illumination conditions remain unchanged for all detection angles. The three-dimensional plot in Fig. 7 summarizes the angle and spectral distribution of the scattered light intensity. It shows the splitting of the single valley, which corresponds to the (111) band gap at $\alpha<20°$, into two valleys at $\alpha>20°$. The light intensity at small angles decreases to shorter wavelengths with the rate $I\propto\lambda^q$, where q drops from $q\approx3.3$ in a straight light to $q\approx0.6$ in scattered light at $\alpha=0°$ and 20°, respectively. At angles α larger than 20° the exponent q changes its sign and acquires values in the interval $q=-0.3$ to -0.6. In this angle range only scattered photons approach the detector. A rapid drop of the transmission with increasing wavelength due to Rayleigh scattering is characteristic for bulk opals [17]. In our opinion, this is not the case with thin opal films, where the strongest scattering occurs at wavelength-scale defects [8]. Moreover, if the scattering were of an isotropic Rayleigh nature, then the strong increase of the scattered light intensity towards shorter wavelengths would be seen along all scattering directions as a counterpart to intensity losses in the transmitted beam. The weak variation of the scattered light intensity at $\alpha>20°$ for all but the diffraction resonance wavelengths suggests a similar scattering efficiency at a given angle for any wavelength in the examined range, which appears to be the consequence of a wide distribution of defect sizes.

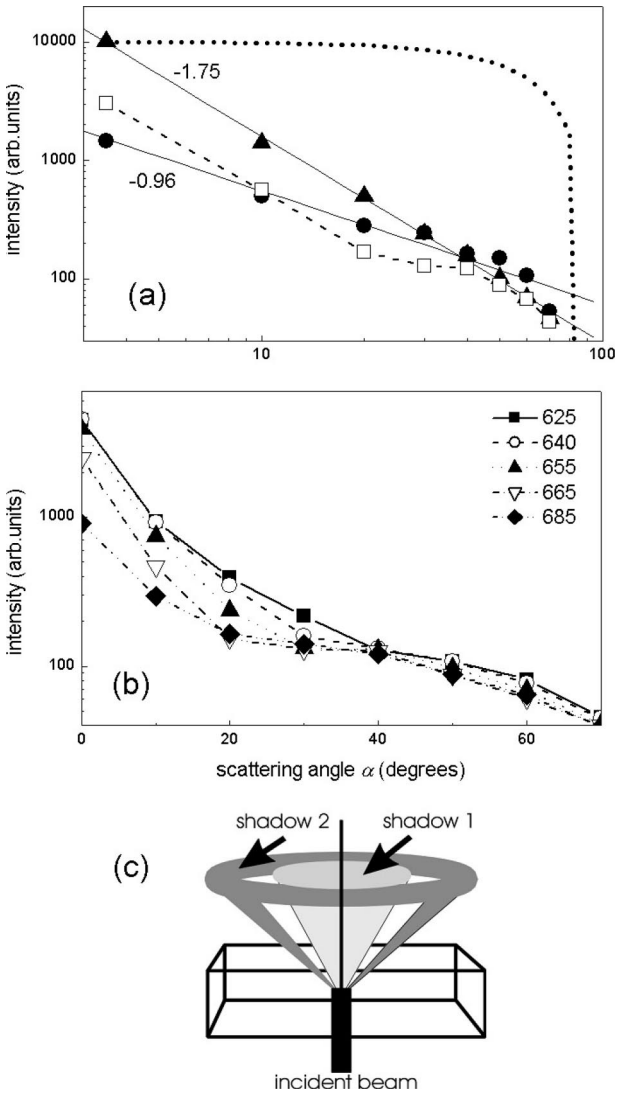

FIG. 8. (a) The FS1 scattering intensity at 500 nm (circles), 662 nm (open squares), and 800 nm (triangles) as a function of the detection angle in double logarithm coordinates. The solid lines are linear fits to experimental data. Numbers at curves show the exponent m in the expression $I\propto I_0\theta^m$. The plateau of the 662-nm plot corresponds to the PBG angle width. The dotted line shows the cos α angle diagram of the Lamberth law as a reference. (b) Evolution of the plateau with the wavelength. (c) Schematics of the PBG projection behind the opal film on the scattering diagram for a given wavelength, which matches both minima. Shadow 1 (2) depicts the angle range of nondispersive (dispersive) minimum. The separation between two shadows is inflated for clarity.

The scattered light intensity drops rapidly with increasing angle α. At wavelengths longer than 800 nm, i.e. above the (111) band gap, this decrease is as fast as $I\propto I_0/\alpha^2$, whereas for shorter wavelengths, e.g., at $\lambda=500$ nm, the drop rate is $I\propto I_0/\alpha$ (Fig. 8). Remarkably, the diagrams follow the same slope throughout the transition angle range from purely transmitted to scattered light [Fig. 8(a)]. The change from an inverse square to a more isotropic inverse linear dependence

occurs gradually over the band gap range. Both functions show a much faster decay of intensity with increasing angle compared to the Lamberth law (Fig. 8). This means that the scattering mechanism strongly favors the forward scattering. This behavior correlates the above assumption concerning the resonant character of scattering in thin opal films.

If the wavelength falls in the PBG, as shown by $\lambda = 662$ nm plot in Fig. 8(a), the intensity vs angle plot demonstrates a plateau spanning over the angle range covered by the diffraction resonance at this wavelength. For any particular wavelength between 700 and 600 nm, i.e., within the PBG range, the directionality diagram peaks along the film normal, which is in fact the direction of the incident beam, then it drops rapidly until it reaches the angle range of nearly constant intensity and then falls again [Fig. 8(b)]. It is worth noting that the bandgap-induced suppression of the light intensity at 685 nm, which is close to the PBG center along [111] axis, starts from $\alpha = 0°$, but the plateau is observed for angle larger than 40° because the long wavelength minimum is not dispersive (see Fig. 3). Alternatively, the angle position and width of the plateau become functions of the wavelength, if this wavelength is in the range of a dispersive minimum. The radial intensity distribution induced by the dispersive minimum can be associated with remnants of the Kossel line, which is the projection of the (111) band gap on the plane behind the opal in the case of divergent monochromatic illumination [1]. In our case, this becomes possible due to the conversion of the collimated beam into a divergent one by scattering. The nondispersive minimum superimposes another shadow on this projection, leading to a complication of the scattering diagram [Fig. 8(c)]. Thus, defects transform a directed beam into a divergent one and form the overall shape of the scattering diagram, whereas the mode structure of the PhC gives rise to the radial modulation of this diagram.

The depth of the minimum in the scattering and transmission spectra of opals is a function of the disorder. Modeling predicts that PBG minima in both components become less pronounced with increasing disorder, but the attenuation dies faster in the diffuse light [16]. With respect to our experiment, the increase of the optical path for larger angles brings about more scattering and, eventually, leads to a change in the scattering regime, when the path length exceeds the MFP. To compare transmission and scattering spectra, the relative depth $\Delta I/I$ of the diffraction minimum was estimated as the ratio of the intensity drop at the band gap center ΔI to the intensity I at the same wavelength without the minimum. The latter value was obtained by extrapolating the spectrum slope (inset to Fig. 9). Plotting $\Delta I/I$ values as a function of the angle in the case of the transmission, one can see that the relative depth changes slowly up to $\theta \leqslant 40°$ and then decreases more rapidly. In contrast, the band gap attenuation in the FS1 spectrum degrades almost linearly with increasing angle over the whole angle range (Fig. 9). It is noteworthy that the relative depth of dips in FS1, FS2, and FS3 spectra is approximately the same [compare Figs. 4(a), 5, and 6], since small differences can be a consequence of dissimilar illumination conditions.

The fact that the disorder-induced degradation of the transmission minimum occurs, predominantly, due to the decrease of the PhC transmittance in allowed bands while the PBG transmittance remains the same [16,18] explains the $\Delta I/I$ behavior in the opal film. This is a consequence of the relatively short Bragg attenuation length, which remains less than the MFP even after changing from the weak to the multiple scattering regime. In particular, an attenuation length of ~ 2 μm was deduced from the 5.7% relative bandwidth of the Bragg resonance in reflectance [19]. The rapid collapse of the band gap attenuation in transmission at $\alpha > 40°$ is associated with the disappearance of the bandgap attenuation for the *p*-polarized light in the vicinity of the Brewster angle [20], which in turn opens a bypass for an essential fraction of unpolarized light to go through the opal film. In contrast, the monotonic decrease of the relative band gap attenuation in the FS1 spectrum with scattering angle reflects the shift of the balance between weakly and multiple scattered photons of PBG wavelengths in the detected flux in favor of the latter due to the respective increase of the optical path in the film.

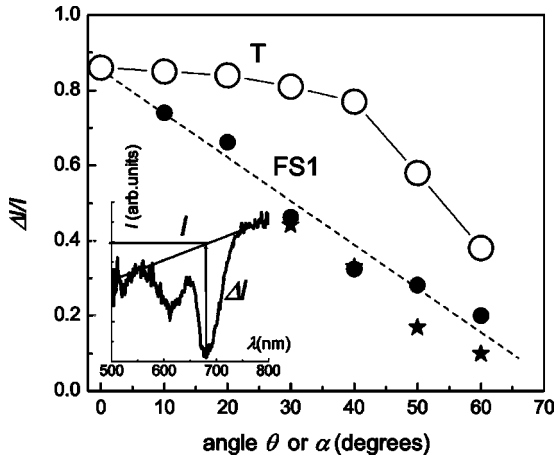

FIG. 9. The relative bandgap attenuation as a function of the corresponding angle in the transmission spectrum (open circles) in comparison with relative long- and short-wavelength minima in the FS1 spectrum denoted by circles and stars, respectively. The inset shows the definition of I and ΔI values for the FS1 spectrum.

The ratio of the full width at half maximum (FWHM) to its central wavelength is 8.6% in transmission along the [111] axis. The estimated bandwidth exceeds the theoretical value of 6.3% obtained from PBG calculations by plane wave expansion method [21], which results from the finite film thickness and the presence of defects [12]. It is worth noting that the relative bandgap FWHM in scattering spectra is less than in transmission in spite of the smaller $\Delta I/I$. For example, the relative bandwidth of the Gaussian fit to the dispersive minimum in transmission at $\theta = \alpha = 40°$ is 11.5% versus 8.2%, 7.3%, and 6.2% values in FS1, FS2, and FS3 spectra at corresponding angles, respectively. Moreover, this observation correlates the apparent squeezing of the bandgap-related minimum in FS1 spectra with respect to the minimum in transmission at small scattering angles (Fig. 3). To understand this phenomenon, comparative studies of the scattering in samples with different disorder are necessary.

V. SUMMARY

The structure of optical modes in thin opal films with low defect density is similar to that of the opal without defects.

This means that each scattering event can be interpreted as photon coupling from one opal eigenmode to another, as suggested by 2D modeling [16]. In other words, the scattered photon is effectively the one which is emitted by the secondary point light source to an opal eigenmode. If photons that experience a single scattering event, as opposed to multiply scattered photons, make up a sufficient portion of the light flux propagating along a direction other than the incident one, the scattered light bears features of the PBG structure.

In general, two minima were observed in the spectra of the scattered light, one of them has been ascribed to the PBG attenuation of the incident beam and the other to the PBG attenuation along the detection direction. Depending on whether the incident or detection direction is the variable, the corresponding minimum changes its central wavelength. Another minimum stays at the wavelength, in agreement with the invariable propagating direction. If the directions of incident and detected light are the same with respect to the [111] axis of the opal lattice, these minima merge into one.

The difference between the light detected in the transmission and scattering configurations is the lost correlation with the wave vector of the incoming beam for the latter. This allows the scattered light to probe all available modes of a PhC. Apparently, the PBG parameters derived from the light scattered in incomplete PhC, like the band gap central wavelength and band gap width, depth, and angular dispersion, represent a close approximation to the parameters of the band gap-induced modification of the spontaneous emission from light sources embedded in an opal film.

The PBG attenuation and the interplay of the MFP and the opal thickness are not the only parameters governing the scattering. We can also point to the characteristic size of defects, which defines the scattering directionality if resonant conditions are achieved. On the one hand, the light scattered in thin opal films demonstrates a pronounced anisotropy, which can be assigned to the resonance scattering at defects of a wavelength scale. On the other hand, the directionality of the scattered light becomes a function of the availability of opal optical eigenmodes. As observed in this work, the effect of defects is to give preference to forward scattering of the light, whereas the PBG effect appears as a suppression of the scattering along the projection of the (111) band gap.

Our results represent a clear experimental demonstration of PBG-related features in the forward scattered light. To achieve a deeper understanding an adequate theoretical model, which is able to account for the scattering at particular lattice defects in conjunction with a consideration of opal dispersion surfaces, needs to be developed.

ACKNOWLEDGMENTS

The authors are grateful to D.N. Chigrin and R. Kian for helpful discussions. The support from the DFG program "Photonic Crystals" SPP1113, EU IST project FUNLIGHT No. 2001-38195, and RFBR Grant No. 02-02-17685 is gratefully acknowledged.

[1] I. I. Tarhan and G. H. Watson, Phys. Rev. B **54**, 7593 (1996).
[2] V. G. Balakirev, V. N. Bogomolov, V. V. Zhuravlev, Y. A. Kumzerov, V. P. Petranovskii, S. G. Romanov, and L. A. Samoilovich, Crystallogr. Rep. **38**, 348–353 (1993).
[3] Yu. A. Vlasov, M. Deutsch, and D. J. Norris, Appl. Phys. Lett. **76**, 1627 (2000).
[4] J. Huang, N. Eradat, M. E. Raikh, Z. V. Vardeny, A. A. Zakhidov, and R. H. Baughman, Phys. Rev. Lett. **86**, 4815 (2001).
[5] Yu. A. Vlasov, V. N. Astratov, A. V. Baryshev, A. A. Kaplyanskii, O. Z. Karimov, and M. F. Limonov, Phys. Rev. E **61**, 5784 (2000).
[6] V. N. Astratov, A. M. Adawi, S. Fricker, M. S. Skolnick, D. M. Whittaker, and P. N. Pusey, Phys. Rev. B **66**, 165215 (2002).
[7] A. V. Baryshev, A. V. Ankudinov, A. A. Kaplyanskii, V. A. Kosobukin, M. F. Limonov, K. B. Samusev, and D. E. Usvyat, Phys. Solid State **44**, 1648 (2002).
[8] V. G. Solovyev, S. G. Romanov, D. N. Chigrin, and C. M. Sotomayor Torres, Synth. Met. **139**, 601 (2003).
[9] A. F. Koenderink, M. Megens, G. van Soest, W. L. Vos, and A. Lagendijk, Phys. Lett. A **268**, 104 (2000).
[10] Y. Xia, B. Gates, Y. Yin, and Yu Lu, Adv. Mater. (Weinheim, Ger.) **12**, 693 (2000).
[11] J. F. Bertone, P. Jiang, K. S. Hwang, D. M. Mittleman, and V. L. Colvin, Phys. Rev. Lett. **83**, 300 (1999).
[12] J. F. Galisteo-Lopez, E. Palacios-Lidon, E. Castillo-Martinez, and C. Lopez, Phys. Rev. B **68**, 115109 (2003).
[13] M. Müller, R. Zentel, T. Maka, S. G. Romanov, and C. M. Sotomayor Torres, Chem. Mater. **12**, 2508 (2000).
[14] H. Migues, C. Lopez, F. Merseguer, A. Blanco, L. Vazquez, and R. Mayoral, Appl. Phys. Lett. **71**, 1148 (1997).
[15] S. G. Romanov, D. N. Chigrin, V. G. Solovyev, T. Maka, N. Gaponik, A. Eychmüller, A. L. Rogach, and C. M. Sotomayor Torres, Phys. Status Solidi A **197**, 662 (2003).
[16] M. A. Kalitieevski, J. Manzanares-Martinez, D. Cassagne, and J. P. Albert, Phys. Rev. B **66**, 113101 (2002).
[17] Y. A. Vlasov, M. A. Kaliteevski, and V. V. Nikolaev, Phys. Rev. B **60**, 1555 (1999).
[18] M. Golosovsky, Y. Neve-Oz, and D. Davidov, Synth. Met. **139**, 705 (2003).
[19] S. G. Romanov, T. Maka, C. M. Sotomayor Torres, M. Müller, and R. Zentel, J. Appl. Phys. **91**, 9426 (2002).
[20] S. G. Romanov, D. N. Chigrin, and C. M. Sotomayor Torres (unpublished).
[21] S. G. Romanov, T. Maka, C. M. Sotomayor Torres, M. Müller, R. Zentel, D. Cassagne, J. Manzanares-Martinez, and C. Jouanin, Phys. Rev. E **63**, 056603 (2001).